

TECHNICAL REPORT No. 20

TO

THE OFFICE OF NAVAL RESEARCH
CONTRACT No. N00014-76-C-0037, NR 031-756

THE EFFECT OF HYDROGEN ON THE MULTIAXIAL
STRESS-STRAIN BEHAVIOR OF TITANIUM TUBING

C. W. LENTZ AND D. A. KOSS
DEPARTMENT OF METALLURGICAL ENGINEERING
MICHIGAN TECHNOLOGICAL UNIVERSITY
HOUGHTON, MICHIGAN

AND

M. G. STOUT AND S. S. HECKER
LOS ALAMOS NATIONAL LABORATORY
LOS ALAMOS, NEW MEXICO

DTIC FILE COPY

ADA 128996

DTIC
ELECTE
JUN 8 1983
S D

REPRODUCTION IN WHOLE OR IN PART IS PERMITTED FOR ANY
PURPOSE OF THE UNITED STATES GOVERNMENT. DISTRIBUTION
OF THIS DOCUMENT IS UNLIMITED.

88 06 06 058

REPORT DOCUMENTATION PAGE		READ INSTRUCTIONS BEFORE COMPLETING FORM	
1. REPORT NUMBER No. 20		2. GOVT ACCESSION NO. A128 996 3. RECIPIENT'S CATALOG NUMBER	
4. TITLE (and Subtitle) The Effect of Hydrogen on the Multiaxial Stress-Strain Behavior of Titanium Tubing		5. TYPE OF REPORT & PERIOD COVERED	
7. AUTHOR(s) C. W. Lentz, D. A. Koss, M. G. Stout, and S. S. Hacker		6. CONTRACT OR GRANT NUMBER(s) N00014-76-C-0037 NR 031-756	
8. PERFORMING ORGANIZATION NAME AND ADDRESS Department of Metallurgical Engineering Michigan Technological University Houghton, MI 49931		10. PROGRAM ELEMENT, PROJECT, TASK AREA & WORK UNIT NUMBERS	
11. CONTROLLING OFFICE NAME AND ADDRESS Office of Naval Research 800 N. Quincy Street Arlington, VA 22217		12. REPORT DATE March, 1983	
14. MONITORING AGENCY NAME & ADDRESS (if different from Controlling Office)		13. NUMBER OF PAGES 24	
		15. SECURITY CLASS. (of this report) Unclassified	
		15a. DECLASSIFICATION/DOWNGRADING SCHEDULE	
16. DISTRIBUTION STATEMENT (of this Report) Distribution of this document is unlimited.			
17. DISTRIBUTION STATEMENT (of the abstract entered in Block 20, if different from Report)			
18. SUPPLEMENTARY NOTES			
19. KEY WORDS (Continue on reverse side if necessary and identify by block number) Deformation, multiaxial stress-strain behavior, titanium, hydrogen			
20. ABSTRACT (Continue on reverse side if necessary and identify by block number) The influence of internal hydrogen on the multiaxial stress-strain behavior of commercially pure titanium has been studied. Thin-walled tubing specimens containing either 20 or 1070 ppm hydrogen have been tested at constant stress ratios in combined tension and internal pressure. The addition of hydrogen lowers the yield strength for all loading paths but has no significant effect on the strain hardening behavior at strains $\epsilon > 0.02$. Thus, the hydrogen embrittlement of titanium under plain strain or equibiaxial loading is not			

a consequence of changes of flow behavior. The yielding behavior of this anisotropic material is described well by Hill's quadratic yield criterion. As measured mechanically and by pole figure analysis, the plastic anisotropy changes with deformation in a manner which depends on stress state. Hill's criterion and the associated flow rule do not describe the multiaxial flow behavior well because of their inability to account for changes of texture which depend on multiaxial stress path. Hence, a strain dependent, texture-induced strengthening effect in equibiaxial tension is observed, this effect having the form of an enhanced strain hardening rate.

Accession For	
NTIS GRA&I	<input checked="" type="checkbox"/>
DTIC TAB	<input type="checkbox"/>
Unannounced	<input type="checkbox"/>
Justification	
By	
Distribution/	
Availability Codes	
Dist	Avail and/or Special
A	



The Effect of Hydrogen on the Multiaxial
Stress-Strain Behavior of Titanium Tubing

C. W. Lentz and D. A. Koss
Department of Metallurgical Engineering
Michigan Technological University
Houghton, Michigan

and

M. G. Stout and S. S. Hacker
Los Alamos National Laboratory
Los Alamos, New Mexico

ABSTRACT

The influence of internal hydrogen on the multiaxial stress-strain behavior of commercially pure titanium has been studied. Thin-walled tubing specimens containing either 20 or 1070 ppm hydrogen have been tested at constant stress ratios in combined tension and internal pressure. The addition of hydrogen lowers the yield strength for all loading paths but has no significant effect on the strain hardening behavior at strains $\epsilon \geq 0.02$. Thus, the hydrogen embrittlement of titanium under plain strain or equibiaxial loading is not a consequence of changes of flow behavior. The yielding behavior of this anisotropic material is described well by Hill's quadratic yield criterion. As measured mechanically and by pole figure analysis, the plastic anisotropy changes with deformation in a manner which depends on stress state. Hill's criterion and the associated flow rule do not describe the multiaxial flow behavior well because of their inability to account for changes of texture which depend on multiaxial stress path. Hence, a strain dependent, texture-induced strengthening effect in equibiaxial tension is observed, this effect having the form of an enhanced strain hardening rate.

INTRODUCTION

Many studies have shown that tensile ductility and fracture resistance of Ti alloys often degrade with increasing hydrogen content. In the case of commercial pure (CP) Ti, the embrittlement effects under uniaxial loading conditions are generally pronounced only at high strain rates, low temperatures, or in the presence of notches.¹⁻⁷ Recent evidence also indicates that hydrogen embrittlement of CP Ti is sensitive to the stress state. Although no loss of ductility occurs in CP Ti sheet at low strain rates in uniaxial tension, Bourcier and Koss observe a substantial ductility loss due to hydrogen embrittlement of sheet specimens deformed in plane strain or equibiaxial tension⁸. The mechanism responsible for this sensitivity of hydrogen embrittlement to multiaxial stress states is not established. One obvious possibility is that hydrogen affects the strain hardening behavior under multiaxial loading such that this induces or contributes to the observed loss of ductility. Thus, the purpose of this study is to examine the effects of internal hydrogen on the multiaxial stress-strain behavior of CP Ti tubing. The influence of hydrogen as well as stress state on the yield and flow stresses and strain hardening behavior will be determined and examined with respect to hydrogen-induced embrittlement. It should be noted that the experimental behavior of the uncharged tube specimens relates to, but differs from, previous multiaxial deformation studies of CP Ti sheet: that of Mullins and Patchett⁹ on very anisotropic, coarse-grained high purity Ti which twins readily and those of Lee and Backofen¹⁰ on Ti sheet of comparable purity but with basal-transverse texture resulting in very easy through-thickness slip when stressed in the rolling direction.

EXPERIMENTAL

All specimens were precision-drawn, Ti tubes with oxygen contents which unfortunately varied from tube to tube in the as-received condition. The

tubes were subsequently either annealed in vacuum at a pressure of less than 1.3×10^{-3} Pa or thermally-charged in a controlled pressure of hydrogen gas to an internal hydrogen content of ~ 1070 wt. ppm. Both the annealing and the hydrogen-charging treatments were conducted at 700°C for a period of 75 minutes after which the specimens were cooled in He gas at $\sim 75^\circ\text{C}/\text{min}$. The oxygen contents of the individual specimens are listed in Table I; note that the oxygen contents vary from 1080 to 2000 ppm. Analyses of the hydrogen contents in the test specimens indicated that the annealed specimens contained ~ 20 wt. ppm H while the charged material contained ~ 1070 wt. ppm H. Representative microstructures of the specimens are shown in Fig. 1 and consist of equiaxed, recrystallized grains of $\sim 10 \mu\text{m}$ diameter; this is equivalent to approximately 50 grains through the tube wall. The hydrogen-charged specimens contain titanium hydride particles, as shown in Fig. 1(b). The hydrides are located both along the grain boundaries and within individual grains.

The test specimens consisted of tubes with a 12.7 mm O.D. and a 0.508 ± 0.013 mm wall thickness and which were 254 mm long. The tube tests themselves were performed under proportional (constant stress ratio) loading with flow behavior being determined from yielding to failure. Five loading paths were chosen: axial tension ($\sigma_{\theta\theta} = 0$), diametral plane strain ($\epsilon_{\theta\theta} = 0$), balanced biaxial tension ($\sigma_{zz} = \sigma_{\theta\theta}$), axial plane strain ($\epsilon_{zz} = 0$) and hoop tension ($\sigma_{zz} = 0$). In addition, the plastic strain ratios were continuously monitored. All tests were performed with an electro-hydraulic, servo-controlled axial/internal pressure testing machine described elsewhere.¹¹ Strains were monitored by both three-element strain gage rosettes and axial plus diametral strain gage extensometers. An effective strain rate of $\sim 1 \times 10^{-3} \text{ s}^{-1}$ was employed.

EXPERIMENTAL RESULTS AND DISCUSSION

A. Plastic Anisotropy

Presentation and interpretation of the multiaxial deformation data requires an adequate choice of a yield and flow criterion. This in turn requires a characterization of the crystallographic texture and plastic anisotropy of this hcp Ti alloy. Figure 2 shows that the tube specimens in the present study possess textures in which the basal plane poles tend to align perpendicular to the tube axis in the radial-tangential plane of the tube, while the poles of a prism plane show a tendency to align with the tube axis. As such, the initial textures prior to deformation differ substantially from the basal-transverse texture of the Ti sheet examined by Lee and Backofen¹⁰ or the very strong alignment of basal plane poles in the Mullins and Patchett sheet.⁹

Deformation causes changes in the textures. Figure 3 shows the effects of axial and equibiaxial tensile deformation on both basal and prism pole figures after an equivalent (Hill¹²) strain of approximately 0.14. Compared to the initial pole figures in Fig. 2, Fig. 3 shows that a reorientation of basal planes has occurred with the poles still tending to align in the radial-tangential plane of the tube but with a maximum intensity near the radial direction. The basal pole textures which develop after uniaxial deformation are similar but not identical to those after equibiaxial straining; in particular, the distribution of basal poles is more intense near the radial direction after equibiaxial deformation than after uniaxial deformation (see Fig. 3). The prism pole figures also change with deformation with the prism poles developing a stronger tendency to align with the tube axis after deformation (compare Figs. 2 and 3). Again there are small but distinct differences in the prism pole figures developed after uniaxial deformation when compared to those after equibiaxial straining (see Fig. 3).

Given the crystallography of slip in hcp alloys*, the textures in Figs. 2 and 3 indicate that the tubing should exhibit a degree of plastic anisotropy and that this will change with deformation. Using the conventional parameters R and P as measures of plastic anisotropy ($R = d\epsilon_{\theta\theta}/d\epsilon_{rr}$ and $P = d\epsilon_{zz}/d\epsilon_{rr}$ in the cylindrical coordinate system of a tube of radius r and with an axis along the z direction), Fig. 4 shows the dependence of R and P on axial or hoop tensile strain, respectively. $R \approx 1.0$ for all strains at 20 ppm H and, it turns out, at 1070 ppm H as well. Such a value of R is consistent with the pole figure data in Figs. 2 and 3 if one uses that data to obtain the Kallstrom texture factor¹³ F . It has been shown that F and R can be related by $F = (R-1)/(R+1)$ and that this relationship is well obeyed for Zr alloy tubing.¹⁴ An analysis of the pole figure data in Figs. 2 and 3 does indeed predict $R \approx 1$, the range being $R = 1.0$ (Fig. 2) to $R = 1.2$ (Fig. 3, equibiaxial). In contrast, at the 2000 $\mu\epsilon$ ($\mu\epsilon = 10^{-6}$) yield strain $F = 2.5$ for the 20 ppm H material but 1.7 for the specimens containing 1070 ppm H. Deformation causes the P -values to decrease, but while the Ti-1070 H material is plastically isotropic at $\epsilon \approx 0.05$, the Ti-20 H material retains a significant degree of plastic anisotropy such that $P \approx 1.6$ at $\epsilon = 0.10$.

The moderate decrease in plastic anisotropy which accompanies the presence of hydrides in the Ti-1070 H alloy does not seem to be associated with texture differences. Indeed, the initial textures of the two materials (Ti-20 H vs Ti-1070 H) are identical and thus the 2000 $\mu\epsilon$ P -values should be the same. We are led to speculate that the large hydrides, particularly at grain boundaries (see Fig. 1b), act to reduce the plastic anisotropy. This

*It should be noted that the Ti tested in this study deforms predominantly by slip; the volume fraction of twins remains <3% for all loading paths. This is in contrast to the Ti examined by Mullins and Paochetti which because of lower oxygen content, deformed primarily by twinning.

may be an indirect effect of multiple slip associated both with the plastic zones which accompany hydride formation in Ti alloys^{15,16} and with the plastic incompatibility strains that develop near hydrides upon subsequent deformation. Thus, additional deformation systems are activated, and the plastic anisotropy should decrease.

The final aspect regarding plastic anisotropy is the recognition, based on the pole figure data in Fig. 3, that the plastic anisotropy changes induced by uniaxial tension (Fig. 4) should not be identical to those induced by equibiaxial straining. Although the difference is not great, Fig. 3 shows that, when compared to uniaxial straining, equibiaxial deformation results in a greater intensity of basal poles concentrated near the radial direction of the tube. Since the slip vectors for basal, prism, and pyramidal slip is contained in the basal plane, this qualitatively means that equibiaxial deformation results in somewhat more difficult through-thickness slip (and therefore a greater degree of plastic anisotropy) than does uniaxial deformation. This is confirmed by previously discussed calculations of R-values based on the Kallstrom texture factor¹⁴ and by an estimate of the P-values defining a Kallstrom factor F' in the radial-axial plane of the tube and assuming, analogous to the expression for R, $F' = (P - 1)/(P + 1)$. The expressions indicate that the "effective" R- and P-values after prestraining in equibiaxial tension should be at least 10% greater than those determined in uniaxial tension (and shown in Fig. 4).

B. Yielding Behavior

Figures 5 and 6 show the experimentally determined yield loci at 2000 μ e for the Ti-20 ppm and Ti-1070 ppm H tube specimens, respectively. The local curvature of the yield surface as determined from experimental measurements of plastic strain vector normality is also shown by the short bar through the data points. A problem encountered in analyzing the raw data is the

specimen-to-specimen variability of the oxygen content (Table I) which was present in the as-received tubes. Previous work has shown that 100 ppm O (by weight) increases the uniaxial yield and ultimate tensile stresses of Ti bar stock by 9-10 MPa and that this increase in stress with oxygen was roughly linear in the range 1000-2000 ppm.^{17,18} Examination of the present data on an effective stress basis shows that an increase of 100 ppm oxygen increases the Hill effective stress by about 10 MPa. Thus data for both yield and flow stresses has been adjusted to a "constant" oxygen content of 1000 ppm using a 10 MPa/100 ppm O factor. The arrows linking some data points in Figs. 5 and 6 indicate the adjustments made to normalize the results to the 1000 ppm O level.

The data in Figs. 5 and 6 shows that the yield stress in pure hoop tension exceeds that in pure axial tension by about 10% at both levels of hydrogen. This observation plus the moderate degree of initial plastic anisotropy measured ($R = 1$, $P = 2.5$ or 1.7) indicates the necessity of an anisotropic yield criterion to predict the yield locus. Thus, Figs. 5 and 6 present a comparison of two commonly used yield criteria (von Mises and the quadratic Hill¹²) to the experimental data for the Ti at both 20 and 1070 ppm H. As seen, the original Hill criterion provides good agreement with experimental data. On the other hand, the yield locus predicted by the von Mises criterion differs considerably in shape from that observed experimentally. Despite the poor agreement between the shapes of the experimental and von Mises yield loci, the differences in the magnitudes between predicted and observed yield stress loci are $\leq 15\%$. The more recent, non-quadratic Hill yield criterion¹⁹ does not allow for normal anisotropy (therefore R and P must have the same value) and is not appropriate. It should also be noted that the yield surfaces in Figs. 5 and 6 differ considerably in shape from those measured by

Lee and Backofen¹⁰ on sheet with $R = 0.4$ and $P = 1.0$ but which also are described quite well by the original, quadratic Hill criterion.¹²

A comparison of the yield surfaces at 20 vs 1070 ppm (Fig. 5 vs 6) shows that hydrogen lowers the yield stress by $\sim 10\%$ for all loading paths. Such an effect has been observed previously², although not always^{4,5}, in uniaxial tension. As will be seen in the true stress-strain curves, the H-induced softening effect occurs only at small strains near yielding, disappearing by $\bar{\epsilon} = 0.02$. It is known that as a consequence of the $\sim 20\%$ increase in volume with the formation of titanium hydride particles in α Ti¹⁶, the development of plastic zones around the hydrides accompanies their formation.^{15,16} Given the large size and volume fraction of hydrides at 1070 ppm (see Fig. 1b) the hydrided specimens will thus contain a significantly higher initial dislocation density. These dislocations can act both as mobile glide dislocation and as dislocation sources. As such, they may serve to increase the initial mobile dislocation density in the material, which according to the dislocation dynamics of yielding, will lower the yield stress. Alternatively, it may be argued that it is the hydrides themselves that yield first and their constrained deformation contributes at least the yield strain. Titanium hydrides do possess some ductility and, depending on composition, may have a slightly lower yield stress than the Ti matrix.²⁰

C. Stress-Strain Behavior

The stress-strain behavior has been examined as a function of stress state from yielding until tube failure. Representative stress-strain curves are shown in Figs. 7-9. Given the dependence of plastic anisotropy on strain (specifically the P -value), the stress-strain data have been calculated using the Hill quadratic yield criterion, the associated flow rule, and allowing R and P to vary with strain according to Fig. 4. The experimental reproducibility of the data is demonstrated by the equibiaxial curves in Figs. 7 and

8. Note that in Fig. 8, the axial plane strain data is from a single test and may not be reliable; attempts to reproduce this curve failed because of test problems.

Two trends emerge from the data in Figs. 7-9. First, as shown in Fig. 9, for strains of $\bar{\epsilon} \geq 0.02$ hydrogen has little effect on the large-strain strain hardening behavior of Ti prior to the instabilities at $\bar{\epsilon}_H \approx 0.15$ which limit the strains achievable in these tube tests. Any differences in stress-strain behavior which do occur in Fig. 9 because of H content are primarily a result of more rapid strain hardening at small strains. This may be associated with geometrically-necessary dislocations created by flow in the ductile Ti matrix near the hydrides.

When compared to the large loss of ductility due to hydrogen embrittlement in equibiaxial tension⁸, taken as a whole the data in Figs. 5-9 indicate that H has only minor influences on the yielding and flow behavior of Ti for nearly the complete range of loading paths which result in sheet thinning. The stress-strain data in Figs. 7-9 is obtained to levels of strains ($\bar{\epsilon} \approx 0.15$) which are a large portion of the fracture strain ($\bar{\epsilon} \approx 0.20$) observed by Bourcier and Koss for failure of Ti-980 H sheet under equibiaxial tension.⁸ Thus, the previously observed large loss of ductility in equibiaxial tension due to H in CP Ti cannot be ascribed to loss of strain hardening capacity induced by H. The absence of a significant effect induced by H is not entirely surprising since most of the H in a Ti-1000 H alloy is not in solid solution but exists within titanium hydrides which are relatively soft and have some ductility¹⁷. Hence, the embrittlement of Ti under biaxial loading must be directly related to the fracture process and is not a consequence of changes of flow behavior.

The second major trend observed in the stress-strain data in Figs. 7 and 8 is that the apparent rate of strain hardening in equibiaxial tension

exceeds that of the other loading paths at both levels of hydrogen. Fitting the stress-strain curves to a parabolic hardening law ($\sigma = k\epsilon^n$) for $\epsilon \geq 0.01$ confirms that the strain hardening in equibiaxial tension ($n = 0.20$ to 0.23) exceeds, for example, that of uniaxial tension ($n = 0.16$ to 0.17). The basis for such a hardening effect has been described earlier in the discussion on plastic anisotropy: the plastic anisotropy changes caused by uniaxial tension (Fig. 4) are not identical to those caused by equibiaxial tension based on the differences in basal pole figures in Fig. 3. In particular, it was concluded that the effective R- and P-values after pre-straining in equibiaxial tension should exceed those determined for uniaxial tension (Fig. 4). This increased difficulty of through-thickness slip has the effect of increasing the equibiaxial flow stress. Thus, the apparent increase in equibiaxial strain hardening is texture-induced strengthening which depends on strain. Current continuum plasticity theories do not account for changes of textures which depend on the stress state. A Taylor-type crystal plasticity analysis would be required.

SUMMARY

While the addition of 1070 wt. ppm H to CP Ti causes a small reduction in multiaxial yield strength, it has no significant effect on the large strain flow behavior. Specifically, hydrogen causes no significant change in strain hardening in either uniaxial, plane strain, or equibiaxial tension at strains >0.02 . We therefore conclude that the previously observed hydrogen embrittlement effects⁸ of Ti sheet deformed in plane strain or equibiaxial tension must be directly related to the fracture process and is not a consequence of changes of flow behavior.

The yield behavior of the anisotropic Ti tube specimens is predicted well by Hill's original, quadratic yield criterion at both 20 and 1070 wt ppm H. However, subsequent deformation causes changes in the crystallographic textures with the extent of the changes depending on stress state. Thus, the multiaxial flow behavior of the Ti is not predicted well because only those texture changes accompanying uniaxial tension can be incorporated through measurements of R- and P-values. In the present case Hill's criterion and the associated flow rule specifically underestimate the equibiaxial flow stresses at large strains because of strain-dependent, texture-induced strengthening effects. This illustrates the inability of continuum plasticity theories to account for different textures evolving through deformation in different stress states.

ACKNOWLEDGMENTS

The authors are very grateful to R. Boyer of Boeing for the texture determinations, R. Aikin for experimental assistance and K. Chan of Southwest Research Institute for constructive comments on the manuscript. This research was supported by the Office of Naval Research through Contract No. N00014-76-C-0027, NR 031-756 and by the U.S. Department of Energy, Offices of Basic Energy Sciences, Division of Materials Sciences.

REFERENCES

1. C. M. Craighead, G. A. Lenning and R. I. Jaffee, Trans. Met. Soc. AIME, 1952, vol. 194, p. 1317.
2. G. A. Lenning, C. M. Craighead and R. I. Jaffee, Trans. Met. Soc. AIME, 1954, vol. 200, p. 367.
3. R. I. Jaffee, G. A. Lenning and C. M. Craighead, Trans. Met. Soc. AIME, 1956, vol. 206, p. 907.
4. C. J. Beevers, M. R. Warren and D. V. Edmonds, J. Less-Common Metals, 1968, vol. 14, p. 387.
5. C. J. Beevers and D. V. Edmonds, Trans. Met. Soc. AIME, 1969, vol. 245, p. 2391.
6. M. Nishigaki, A. Tanabe, Y. Ito and Y. Moriguchi, in Titanium '80, Science and Technology, H. Kimura and O. Izumi, eds., p. 1663, TMS-AIME, Warrendale, PA, 1980.
7. K. J. Puttlitz and A. J. Smith in Hydrogen Effects in Metals, I. M. Bernstein and A. W. Thompson, eds., p. 427, TMS-AIME, Warrendale, PA, 1981.
8. R. J. Bourcier and D. A. Koss, Scripta Met., 1982, vol. 16, p. 515.
9. S. Mullins and B. M. Patchett, Metall. Trans. A, 1981, vol. 12A, p. 853.
10. D. Lee and W. A. Backofen, Trans. Met. Soc. AIME, 1966, vol. 236, p. 1077 and 1696.
11. M. G. Stout, S. S. Hecker and R. J. Bourcier, J. Eng. Mat'l. Tech. (in print).
12. R. Hill, The Mathematical Theory of Plasticity, p. 318, Clarendon Press, Oxford, 1950.
13. K. Kallstrom, Can. Met. Quart., 1972, vol. 11, p. 185.
14. L.F.P. Van Swam, D. B. Knorr, R. M. Pelloux and J. F. Shewbridge, Metall. Trans. A, 1979, vol. 10A, p. 483.
15. N. E. Paton, B. S. Hickman and D. H. Leslie, Metall. Trans., 1971, vol. 2, p. 2791.
16. N. E. Paton and J. C. Williams in Hydrogen in Metals, I. M. Bernstein and A. W. Thompson, eds., p. 409, Am. Soc. Met., Metals Park, OH, 1974.
17. W. L. Finlay and J. A. Snyder, Trans. TMS-AIME, 1950, vol. 188, p. 277.
18. R. I. Jaffee, H. R. Ogden and D. J. Maykuth, Trans. TMS-AIME, 1950, vol. 188, p. 1261.
19. R. Hill, Math Proc. Comb. Phil. Soc., 1979, vol. 85, p. 179.
20. P. E. Irving and C. J. Beevers, J. Mat'l. Sci., 1972, vol. 7, p. 23.

Table I. The Oxygen Contents of the Test Specimens.

The Letter H Designates Specimens Containing 1070 wt ppm H.
Specimens are Grouped According to Loading Path; see Figs.
5 and 6.

Specimen	1 / H3	11 / H8	4 / H5	2 / H9	9 / H1	14 / H2	3 / H4	10 / H13
Oxygen (wt ppm)	1080 / 1900	1250 / 2000	1900 / 1440	1910 / 1850	1260 / 1040	1940 / 1070	1900 / 1140	1740 / 1090

LIST OF FIGURES

- Fig. 1 - Optical micrographs of: (a) Ti-20 wt ppm H and (b) Ti-1070 ppm H. Note the presence of hydrides primarily located along grain boundaries in (b).
- Fig. 2 - Pole figures showing the textures present in both the Ti-20H and Ti-1070H tubes prior to deformation. TA denotes tube axis and TC denotes tube circumference.
- Fig. 3 - Basal ((a) and (b)) and prism ((c) and (d)) pole figures after an equivalent strain $\bar{\epsilon} = 0.14$ for Ti-20H tubes tested in axial tension ((a) and (c)) and balanced biaxial tension ((b) and (d)).
- Fig. 4 - The dependence of the plastic anisotropy parameters R and P on axial and transverse strain, respectively.
- Fig. 5 - Experimental 2000 $\mu\epsilon$ yield data as compared to yield loci predicted by Hill's quadratic and von Mises' yield criteria. Data is for commercially pure Ti containing 20 wt ppm H and corrected to 1000 wt ppm O.
- Fig. 6 - Experimental 2000 $\mu\epsilon$ yield data as compared to yield loci predicted by Hill's quadratic and von Mises' yield criteria. Data is for commercially pure Ti containing 1070 wt ppm H and corrected to 1000 wt ppm O.
- Fig. 7 - The effective stress-strain curves for commercially pure titanium containing 20 ppm H plotted assuming the quadratic Hill criterion with values of R and P varying with strain as per Fig. 4.

Fig. 8 - The effective stress-strain curves for commercially pure titanium containing 1070 ppm H plotted assuming the quadratic Hill criterion with values of R and P varying with strain as per Fig. 4.

Fig. 9 - A comparison of the effective stress-strain curves (Hill criterion) commercially pure titanium containing 20 or 1070 ppm H.

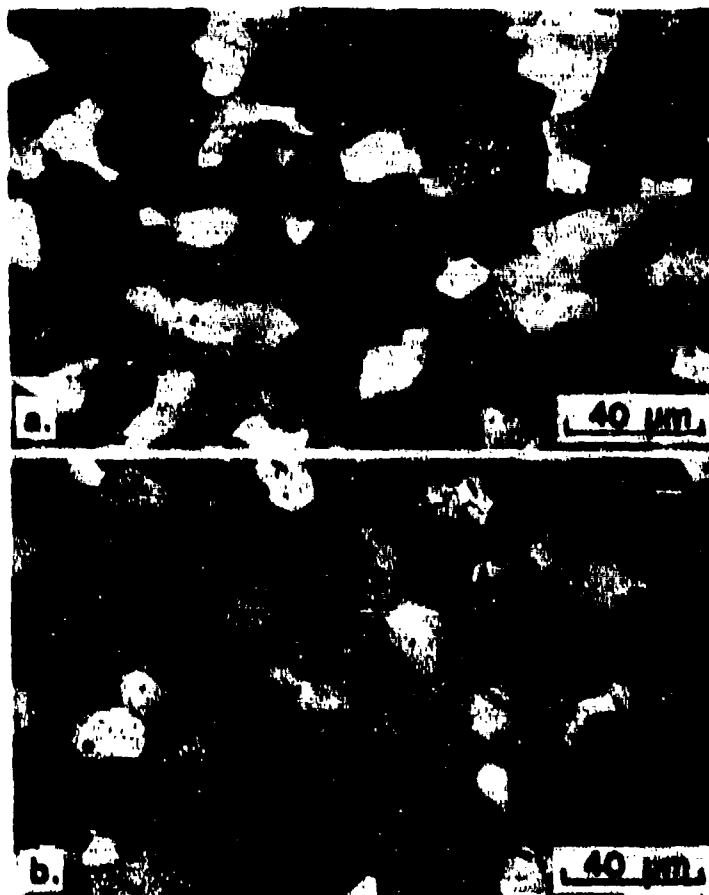


Fig. 1. Optical micrographs of: (a) Ti-20 wt ppm H and (b) Ti-1070 ppm H. Note the presence of hydrides primarily located along grain boundaries in (b).

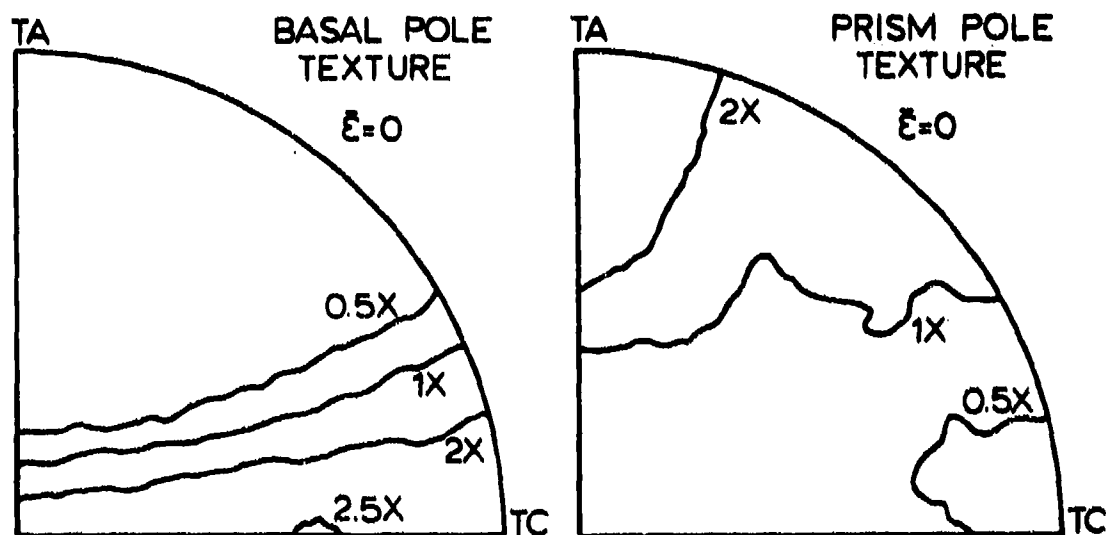


Fig. 2. Pole figures showing the textures present in both the Ti-20H and Ti-1070H tubes prior to deformation. TA denotes tube axis and TC denotes tube circumference.

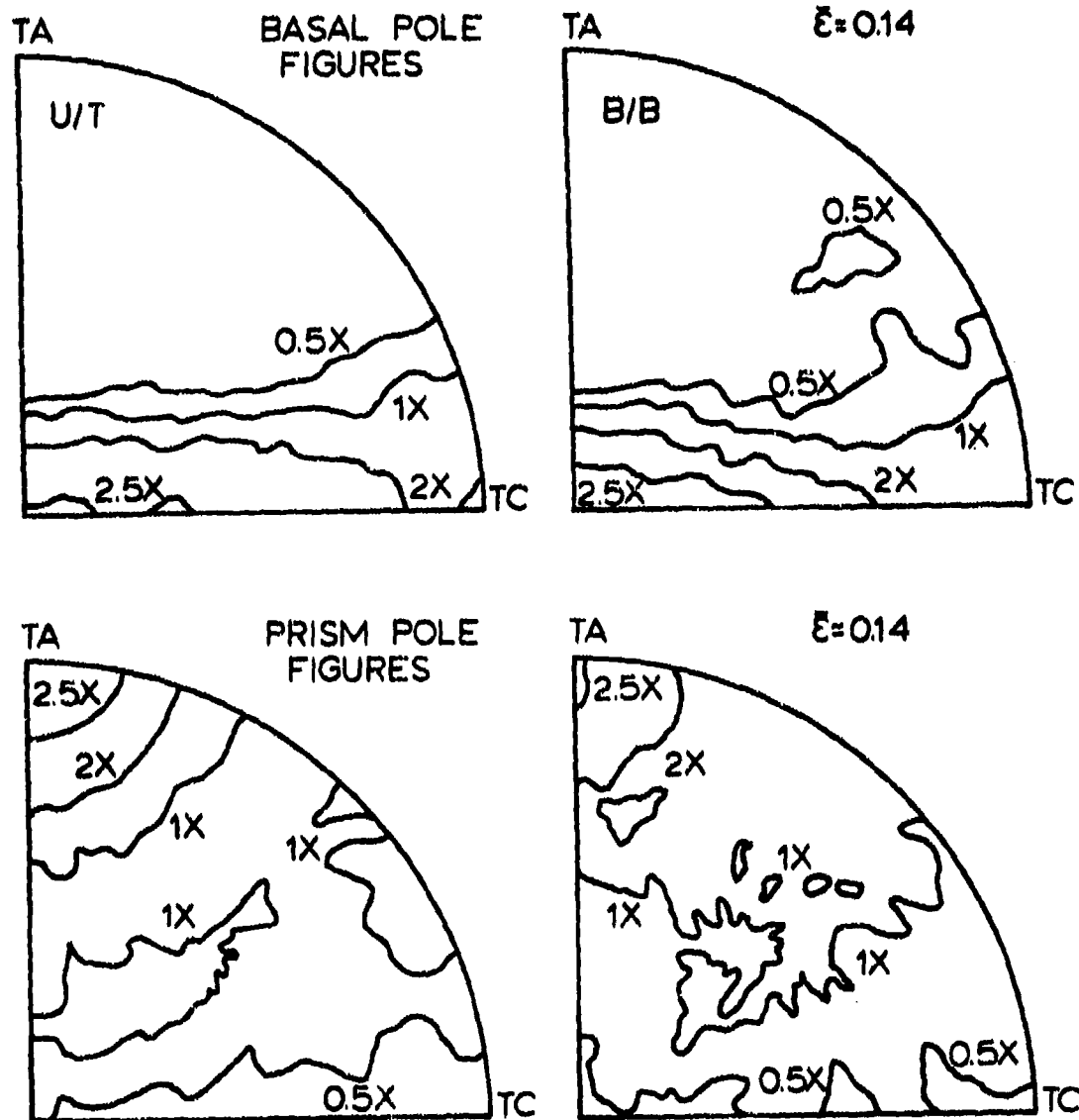


Fig. 3. Basal ((a) and (b)) and prism ((c) and (d)) pole figures after an equivalent strain $\bar{\epsilon} = 0.14$ for Ti-20H tubes tested in axial tension ((a) and (c)) and balanced biaxial tension ((b) and (d)).

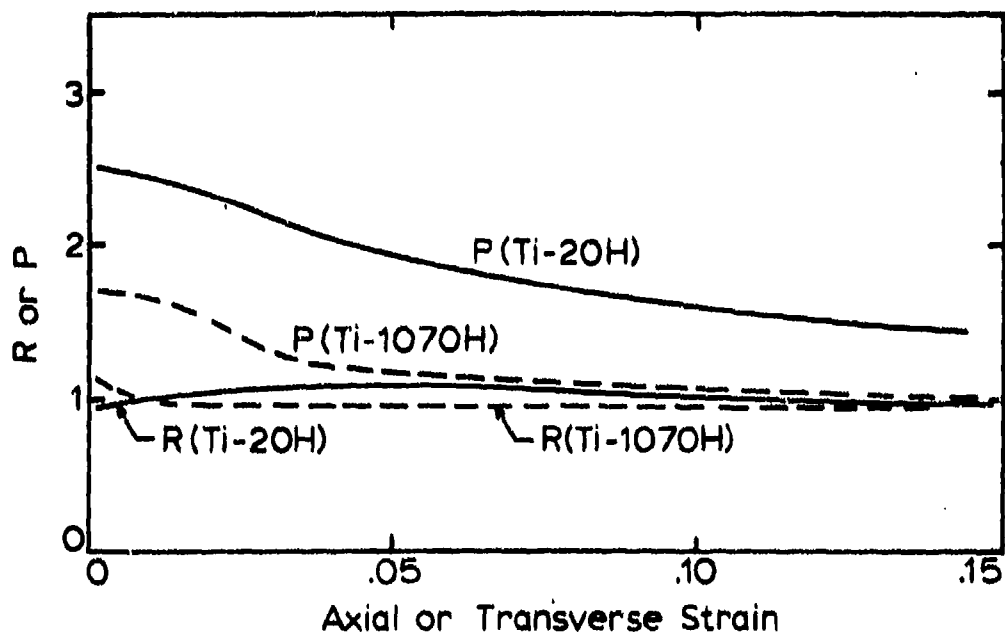


Fig. 4. The dependence of the plastic anisotropy parameters R and P on axial and transverse strain, respectively.

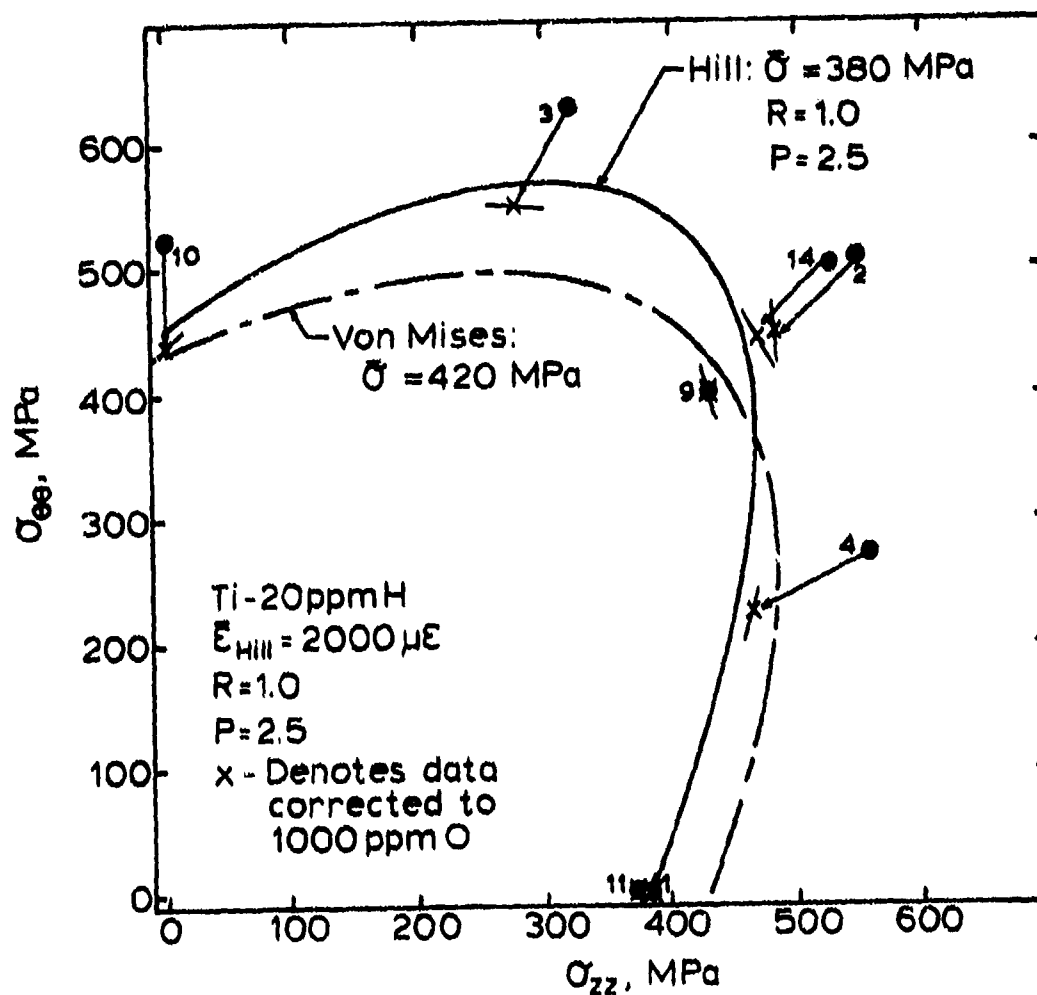


Fig. 5. Experimental 2000 $\mu\epsilon$ yield data as compared to yield loci predicted by Hill's quadratic and von Mises' yield criteria. Data is for commercially pure Ti containing 20 wt ppm H and corrected to 1000 wt ppm O.

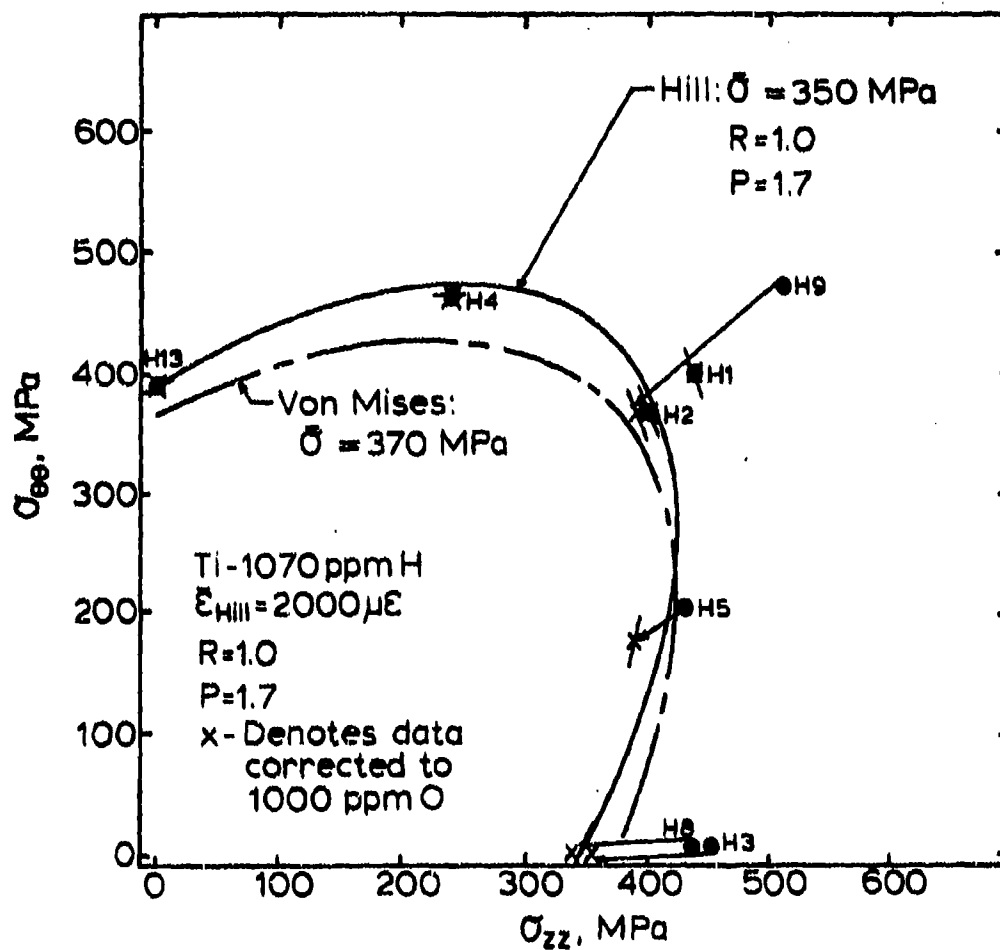


Fig. 6. Experimental 2000 $\mu\epsilon$ yield data as compared to yield loci predicted by Hill's quadratic and von Mises' yield criteria. Data is for commercially pure Ti containing 1070 wt ppm H and corrected to 1000 wt ppm O.

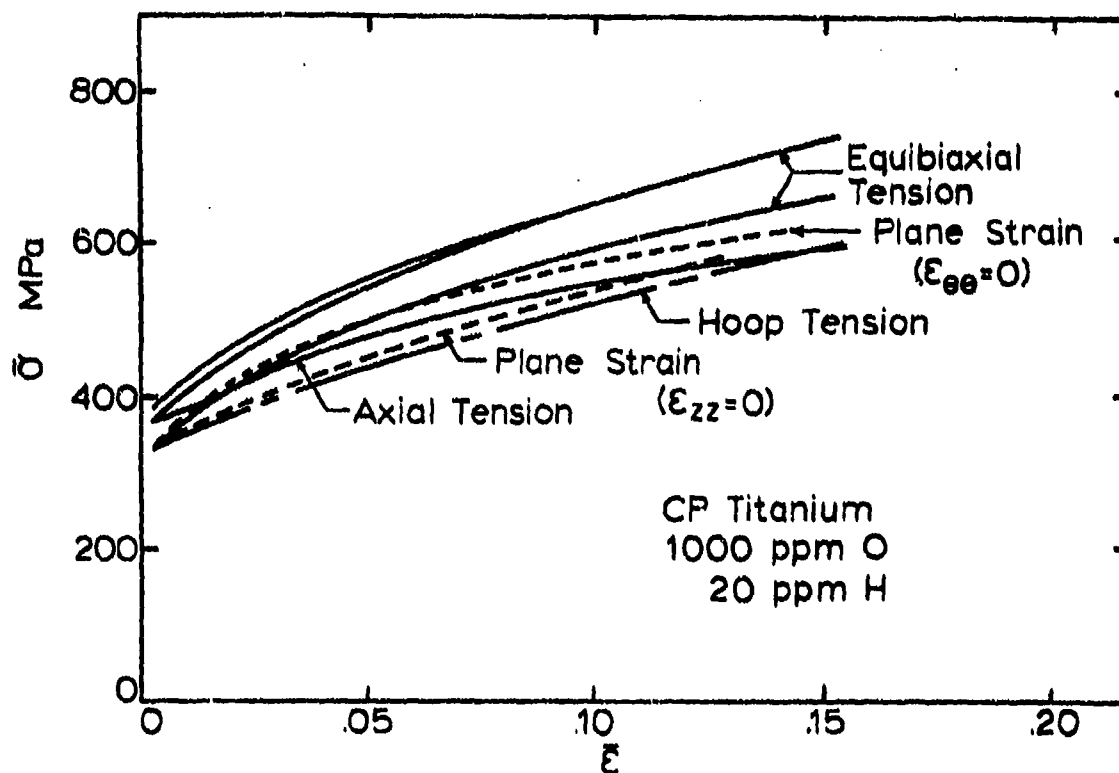


Fig. 7. The effective stress-strain curves for commercially pure titanium containing 20 ppm H plotted assuming the quadratic Hill criterion with values of R and P varying with strain as per Fig. 4.

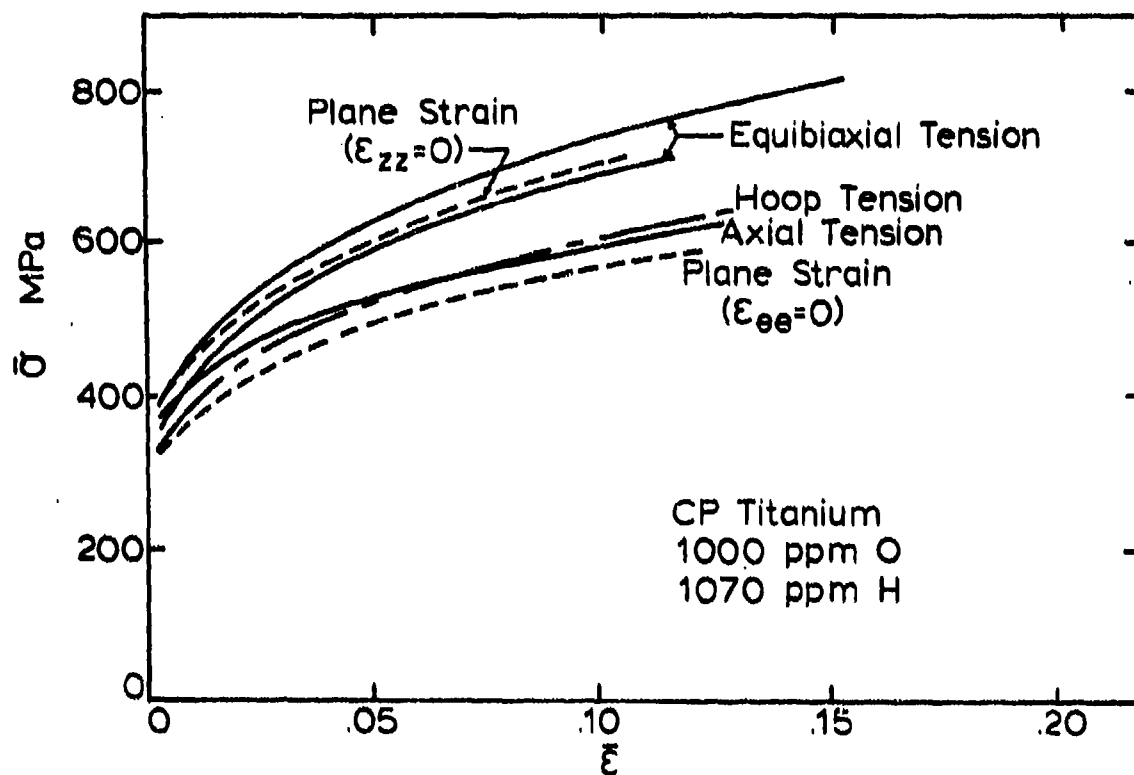


Fig. 8. The effective stress-strain curves for commercially pure titanium containing 1070 ppm H plotted assuming the quadratic Hill criterion with values of R and P varying with strain as per Fig. 4.

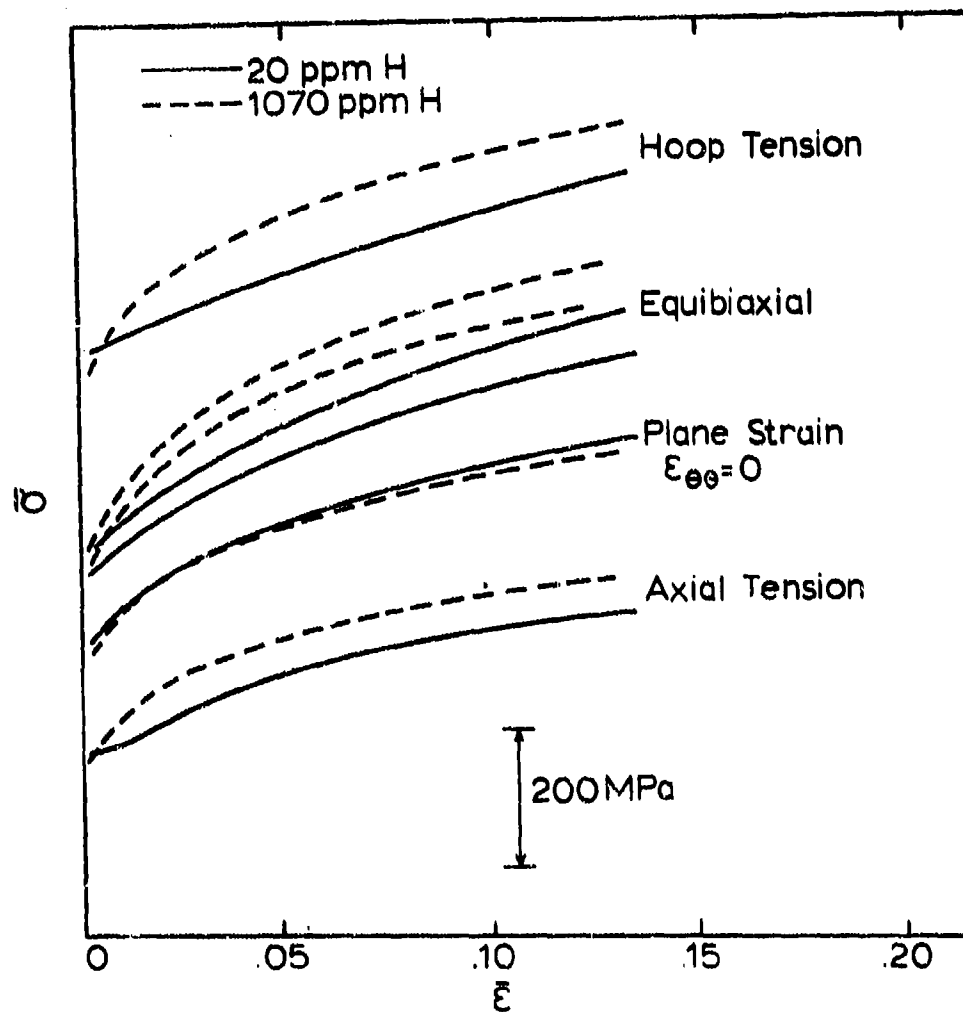


Fig. 9. A comparison of the effective stress-strain curves (Hill criterion) commercially pure titanium containing 20 or 1070 ppm H.